Flexural strengthening of flat slabs with FRP composites using EBR and EBROG methods

Ala Torabian[a,b], Brisid Isufi[b], Davood Mostofinejad[a] and António Pinho Ramos[b,c]

[a]Department of Civil Engineering, Isfahan University of Technology (IUT), Isfahan, Iran

[b]Department of Civil Engineering, Faculty of Science and Technology, Universidade NOVA de Lisboa, Caparica, Portugal

[c]CERIS, Lisbon, Portugal

Corresponding author: Ala Torabian; ala.torabian@cv.iut.ac.ir

E-mail addresses:

ala.torabian@cv.iut.ac.ir (Ala Torabian)

b.isufi@campus.fct.unl.pt (Brisid Isufi)

dmostofi@iut.ac.ir (Davood Mostofinejad)

ampr@fct.unl.pt (António Pinho Ramos)

Abstract

One of the major disadvantages of conventional fibre-reinforced polymer (FRP) strengthening techniques is the premature debonding of the FRP, leading to an underutilization of the materials. The externally bonded reinforcement on grooves (EBROG) method, which has been proven successful in postponing debonding in several structural applications, is examined in this study for the first time for realistic conditions in flat slabs. To this end, two different layouts of the strengthening solution are tested under concentric monotonic loading: one representing roof-level slab-column connections in which carbon FRP (CFRP) sheets are laid on top of the joint region (cross layout); and another one representing intermediate floors, in which the aforementioned layout is not possible due to the presence of the column (grid layout). For each layout, two FRP bonding techniques are used: conventional externally bonded reinforcement (EBR) and EBROG. Another specimen, without FRP strengthening, is used as a reference. It is shown that the EBROG technique is effective in postponing debonding for both layouts. Compared to the specimens in which EBR was used, the load capacity was increased in case of EBROG by 36% when FRP sheets were bonded on top of the joint (cross layout) and by 15% when sheets were attached outside the joint region (grid layout). Debonding strains are shown to be significantly higher in the case of EBROG compared to EBR. The experimentally observed debonding strains were compared with code provisions and predictions of models from the literature. A simple calculation method giving reasonably good results for the load capacity of the FRP-strengthened specimens is presented.

Keywords: Flat slab; EBR; EBROG; CFRP; debonding; concentric loading.

1 Introduction

Reinforced concrete (RC) flat slabs are popular in office and residential buildings worldwide. As with other structural elements in case of changes in occupancy, errors in execution and design or code updates, it is often required to strengthen flat slabs to achieve an acceptable level of safety or to mitigate serviceability issues. Flat slabs can require strengthening against flexure and/or punching shear.

Different solutions for punching shear strengthening of flat slabs have been developed and investigated in several studies. Among these solutions, employing post-installed bolts has been shown to be one of the most efficient [1–6]. Also, using fibre reinforced polymer (FRP) rods, fans, grids, or stirrups has been proven to be sufficiently effective [7–10].

Several solutions have been developed, tested and used for flexural strengthening of existing flat slabs. Methods that result in an increase of the effective depth of the slab are attractive because increasing the effective depth enhances both flexural and punching shear strength, but it is usually accompanied by an increase of the gravity loads and mass of the structure. When the increase of the effective depth is sought on the tensile face, further issues can arise due to the cracked state of the concrete substrate [11]. Fernandes et al. [11] and Lapi et al. [12] studied the efficiency of adding a concrete overlay to strengthen flat slabs. Ebead and Marzouk [13] showed that strengthening of flat slabs via the attachment of steel plates around the column through steel bolts can effectively enhance the behavior of the slab. Fabric reinforced cementitious matrix (FRCM) composites, consisting of fibre textiles and mortar matrix, were used in several studies to strengthen different cases of RC elements including RC slabs [14–19]. Strengthening of two-way RC slabs with FRCM was investigated for increasing the punching shear strength [17,18] as well as for improving the flexural capacity [19].

Besides the aforementioned techniques, a very popular flexural strengthening technique consists of applying FRP on the tension face of the slab using epoxy resin. FRP strengthening has several advantages over other methods. A major advantage is that the FRP composites have a high strength to weight ratio and therefore provide a lightweight strengthening solution in different applications. They can be attached to the tension face of the slab in thin sheets or laminates or they can be embedded into pre-cut grooves on the concrete cover in continuous rods. The installation of FRP composites is relatively simple and quick. This strengthening solution is aesthetic because the thin layers of FRP can be easily covered without changing the dimensions of the strengthened structural elements. Another advantage is that the strengthening technique with FRP does not induce significant damage to the existing structure during installation (there is no risk of destroying the internal reinforcement as a result of drilling holes across the member and no significant concrete removal is involved). A disadvantage of the technique is that it requires careful preparation of the concrete substrate to ensure that proper bonding of the FRP composites is achieved. Another disadvantage is that, in practice, the application of the FRP system can be limited by its relatively low fire resistance. As a result, FRP system can be considered applicable only when adequate fire protection is provided through the floor finishes, coatings, insulation systems, fire retardant (additive to the resin or coating on the surface of the FRP), or when the un-strengthened slab has sufficient capacity to carry the loads for the combination of actions including fire.

The most common method employed for FRP bonding in different structural elements, including two-way slabs, is externally bonded reinforcement (EBR) method in which the weak concrete layers are removed by abrading the surface and FRP composites then adhere directly on the underlying surface. In this method, even under very good concrete substrate conditions, the failure of the strengthened structural element is often governed by debonding of the FRP layer before achieving the ultimate strength of the FRP [20–27]. Providing anchorage systems for the externally bonded FRP composites, such as steel end anchor plates [28], transverse FRP anchorages [20,22], and steel bolts

[29,30], and also using mechanically fastened (MF) FRP technique [25] has been indicated to serve, to a certain extent, in preventing a premature debonding failure.

Near-surface mounted (NSM) technique was introduced as an alternative to the EBR method. In the NSM technique, grooves are cut in the concrete cover and FRP rods are embedded into the grooves with an appropriate adhesive. The effectiveness of flexural and shear strengthening of RC structures, including RC beams, with near-surface mounted FRP rods has been assessed in several studies. The NSM technique was proven to be more efficient than the EBR method since the NSM rods are less sensitive to debonding [31–36]. An investigation on two-way RC slabs strengthened with NSM FRP rods was conducted by Foret and Limam [37], reporting an economic advantage of the NSM technique over the EBR method, relative to a lower carbon fibre quantity.

More recently, a solution, named as Externally Bonded Reinforcement On Grooves (EBROG), has been introduced by Mostofinejad and Mahmoudabadi to improve the bond between the FRP layer and the concrete substrate in concrete beams [38]. This solution was then proven to be a competent substitute for the conventional EBR method in different structural elements (beams [39,40], RC columns [41–43], and beam-column joints [44,45]). EBROG consists of cutting grooves in the concrete cover as surface preparation (without any surface abrading), filling the grooves with epoxy resin as well as applying resin on the concrete surface, and bonding the FRP composites onto the surface on the grooves.

The current research aims to study the effectiveness of CFRP sheets in improving the flexural capacity of flexure-deficient slabs, and to investigate for the first time the efficiency of the EBROG technique in the flexural strengthening of RC slabs with

CFRP sheets, compared with that of the conventional EBR method. Accordingly, the specimens are conservatively strengthened with steel bolts to avoid punching shear failure, which is outside the scope of this study. Indeed, in the case that the ultimate capacity is limited by punching shear failure, investigating the efficiency of various flexural strengthening schemes may not be feasible. Therefore, the bolts were designed so that their employment guarantees avoiding punching shear failure before the exploitation of the flexural capacity of the slab. The employed technique for punching shear strengthening has already been proven efficient in this regard [3]. To achieve the aim of this study, flexural strengthening of flat slabs is performed in two cases: roofs, where CFRP is applicable tothe slab center, and intermediate stories, where column continuity does not allow the application of CFRP over the column region. The concentric loading tests of five flat slab specimens are presented. One specimen without any flexural strengthening serves as a reference specimen. The other four specimens are CFRP strengthened, with two layouts (strengthening over the column region and surrounding the column) and two CFRP bonding methods (EBR and EBROG). No mechanical anchorage is provided in the strengthening systems to allow for a proper investigation of the efficiency of the EBROG technique in preventing premature debonding failure. All the presented specimens are lightly reinforced in flexure, representing a structure that requires flexural strengthening due to increased loading, excessive corrosion of the existing reinforcement, or serviceability issues.

2 Experimental work

2.1 Materials

Ready-mix concrete of grade C30 was used for casting the slabs. The average compressive strength of concrete for each slab specimen, f_c, measured by testing

150×300-mm concrete cylinders on the day of the slab test is given in Table 1. The concrete tensile strength of each specimen, f_{ct}, determined by conducting splitting tensile strength tests is also presented in Table 1. Deformed steel bars with diameter 8 mm were used near the tension face of the slab as top reinforcement and deformed steel bars with diameter 6 mm were placed near the compression face as bottom reinforcement. The 8-mm-diameter bars had yield stress of 538 MPa, ultimate stress of 634 MPa, and a yield strain of 0.27%. The values for the same quantities in the case of 6-mm-diameter bars were 474 MPa, 585 MPa, and 0.24%, respectively. The steel bolts employed for punching shear strengthening of the specimens were M10 with strength grade 8.8.

CFRP composites, made from fibre and matrix phases, were attached to the tension face of the specimens to strengthen them in flexure. The fibre phase consisted of unidirectional carbon fibre fabric S&P C-Sheet 240 with a design thickness of 0.168 mm (Fig. 1), and the matrix phase was epoxy adhesive S&P Resin 55 HP. Mechanical properties of the fabric and the adhesive resin are summarized in Table 2, according to the manufacturer's user guide [46,47].

Fig. 1 Unidirectional carbon fibre fabric S&P C-Sheet 240

Table 1 Specification of test specimens

Specimen	f_c (MPa)	f_{ct} (MPa)	CFRP strengthening configuration	CFRP strengthening technique
REF-B	41.3	2.46	-	-
EBR-CR-B	42.0	3.02	Cross form	EBR
EBROG-CR-B	35.8	2.69	Cross form	EBROG
EBR-GR-B	41.7	2.89	Grid form	EBR
EBROG-GR-B	35.7	2.85	Grid form	EBROG

Table 2 Mechanical properties of CFRP materials [46,47]

Material	Type	Tensile strength (MPa)	Elastic modulus (GPa)	Rupture strain (%)
Fibres	S&P C-Sheet 240	4300	240	1.80
Resin	S&P Resin 55 HP	15.9	3.2	1.73

2.2 Test specimens and test setup

Five RC flat slabs were tested to investigate the performance of the EBROG technique in comparison with the conventional EBR method in two different configurations of flexural CFRP strengthening. For this purpose, all slabs were strengthened with steel shear bolts to prevent a potential punching shear failure which could prevent utilization of the full strength of CFRP composites if it occurred before FRP debonding or rupture. One slab was left without CFRP strengthening to serve as a reference specimen, named as REF-B, and the others were strengthened in flexure with CFRP sheets, using the

EBR method in specimens EBR-CR-B and EBR-GR-B and the EBROG technique in specimens EBROG-CR-B and EBROG-GR-B. The details of the CFRP-strengthened specimens are explained in Section 2.3.

As shown in Fig.2, the overall dimensions of the specimens were 2200×2200×150 mm and the monotonic concentrated load was applied over a steel plate of dimensions 250×250 mm^2 using a hydraulic jack placed centrally under the specimen. The specimens modeled the slab area around an interior column up to the zero bending moment line (Fig.2). The load was applied in a load-controlled manner at a rate of 150 N/s. The slabs were connected to the strong floor using eight strands distributed over the zero bending moment line, connected two by two to four spreader beams which in turn were connected to the strong floor using a threaded bar anchor located at the center of each beam. Each of the strands was equipped with a load cell measuring the applied load. Fig.3 demonstrates a specimen on the test setup.

The specimens had a relatively low flexural reinforcement ratio of 0.2%, simulating flexure-deficient slabs. The 8-mm-diameter top reinforcement bars were placed with a spacing of 190 mm, uniformly distributed over the slab width in both directions. The 6-mm-diameter bottom reinforcement bars were spaced every 190 mm, with the same layout as the top bars. The nominal concrete cover for both top and bottom reinforcement bars was 20 mm. Fig.2 shows the steel reinforcement in the slab section.

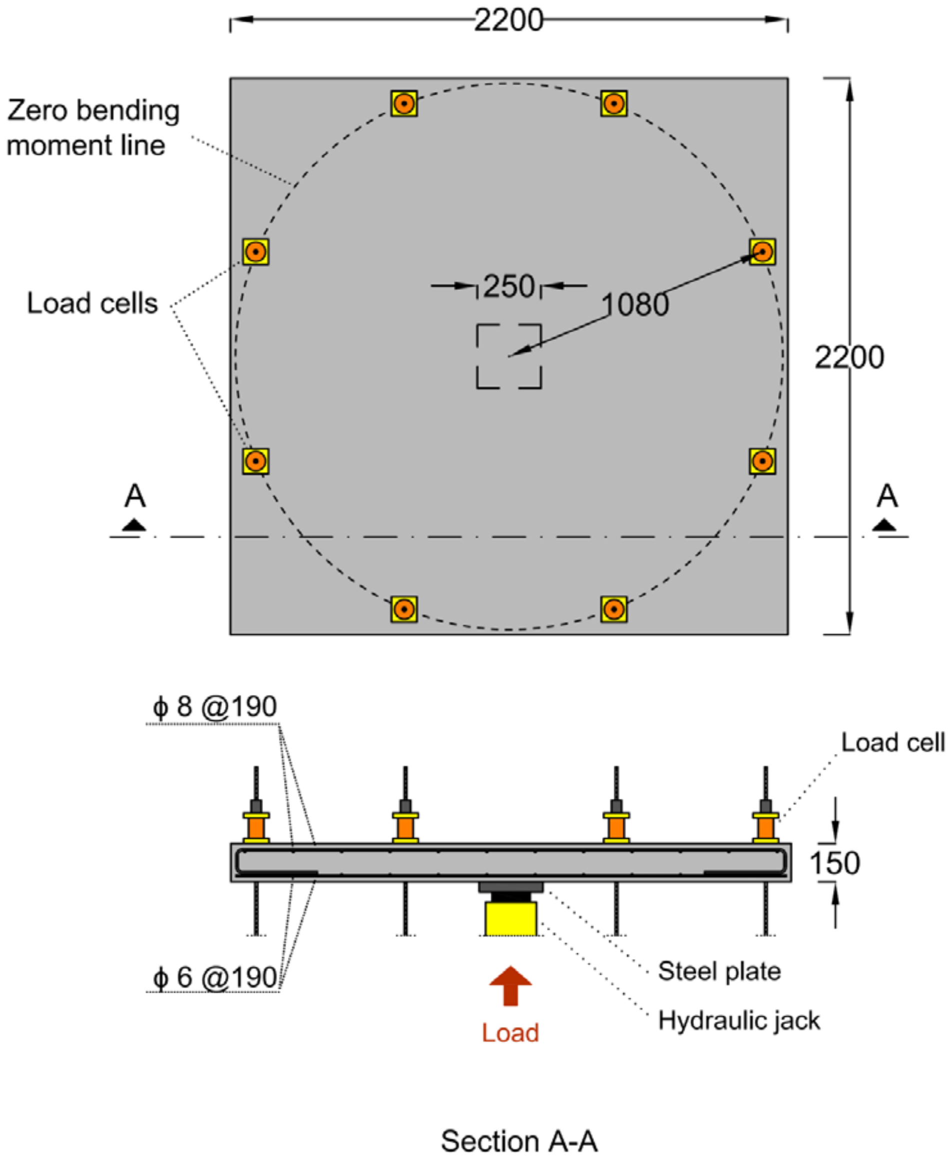

190 Fig.2 Geometry and steel reinforcement of test specimens (dimensions in mm)

Fig.3 Test setup

2.3 Strengthening procedure and designation of the specimens

Table 1 summarizes the CFRP strengthening layouts and techniques used in each specimen. All specimens were strengthened against punching shear failure with forty 10-mm-diameter steel bolts, placed in a radial arrangement in five rows around the column. For this purpose, a rebar scanner was first used to determine the position of flexural reinforcement bars. Holes with a diameter of 12 mm were then drilled in determined places. Finally, the bolts were inserted and tightened with a preload equal to 15.7 kN. The position of the bolts with respect to the column edge and the adjacent bolts is shown in Fig.4a andFig.5a for the specimens with the cross and the grid layout of CFRP strengthening, respectively. Fig.4b and c and Fig.5b and c illustrate section views of the CFRP-strengthened specimens. It should be noted that only the CFRP strips of one direction are sketched in the section views for clarity. As shown in Fig.4a andFig.5a, each CFRP strip consists of two plies of CFRP sheets. The distance between the CFRP strips (Fig.4andFig.5) was provided to make the installation of the steel bolts possible. To strengthen the specimens with both CFRP sheets and steel bolts, the drilled holes were temporarily filled to prevent the entrance of the epoxy resin, and the CFRP sheets were then bonded to the prepared concrete surface. After the final cure of the CFRP composites, the temporary fillers were removed, and the steel bolts were inserted into the holes and tightened.

As can be understood from Fig.4a Fig.5a, the CFRP sheets hindered the unrestricted placement of the bolts. As a result, slightly different layout of bolts in specimens with different CFRP configurations was used. Nonetheless, the perimeter of the shear critical section outside the shear-reinforced zone was the same for both layouts. Each of the bolts was anchored by two circular steel plates with a diameter of 30 mm on the top and bottom of the slab, as shown in Fig.6. The letter B in the shear-reinforced specimens' names ending represents bolts.

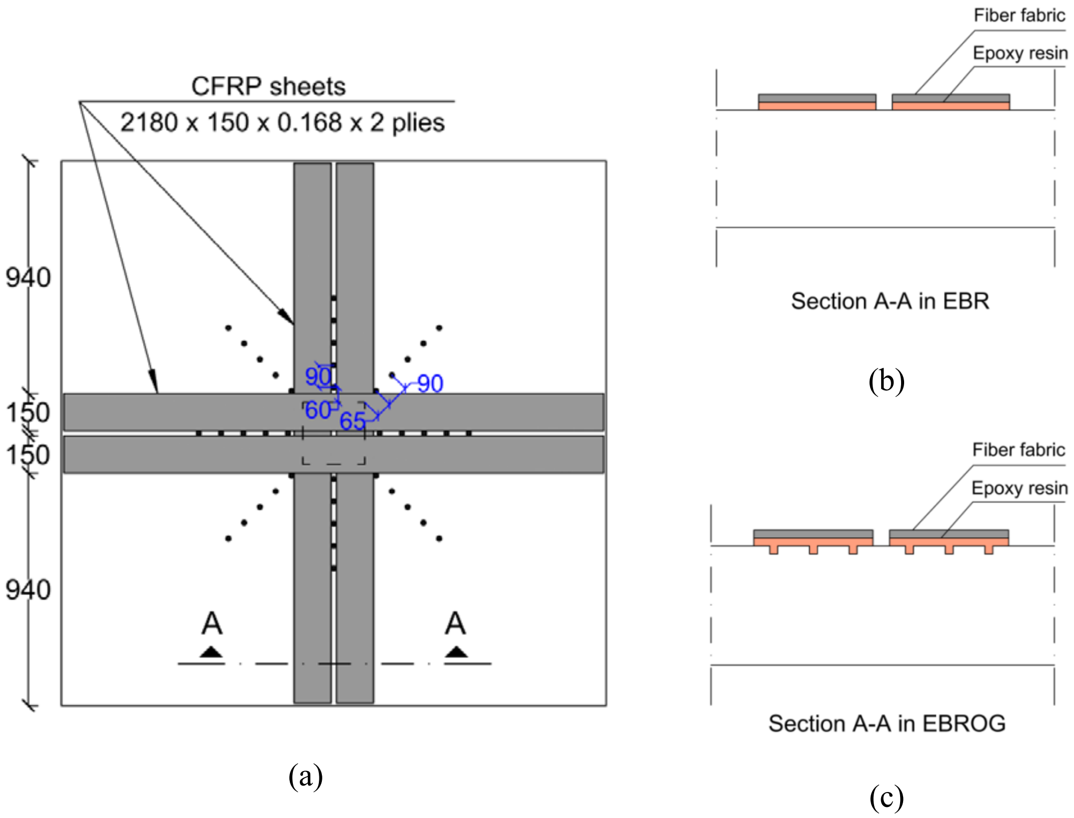

Fig.4 Specimens EBR-CR-B and EBROG-CR-B (dimensions in mm); (a) configuration of CFRP sheets and steel bolts; (b) section view in EBR-CR-B; (b) section view in EBROG-CR-B

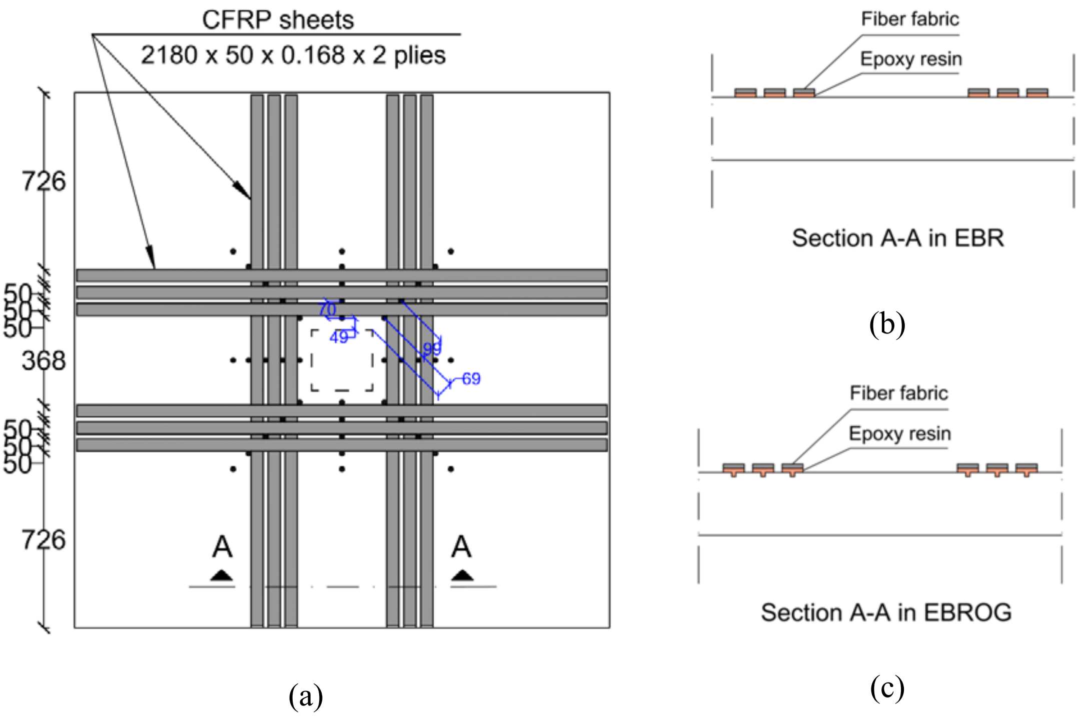

Fig.5 Specimens EBR-GR-B and EBROG-GR-B (dimensions in mm); (a) configuration of CFRP sheets and steel bolts; (b) section view in EBR-GR-B; (c) section view in EBROG-GR-B

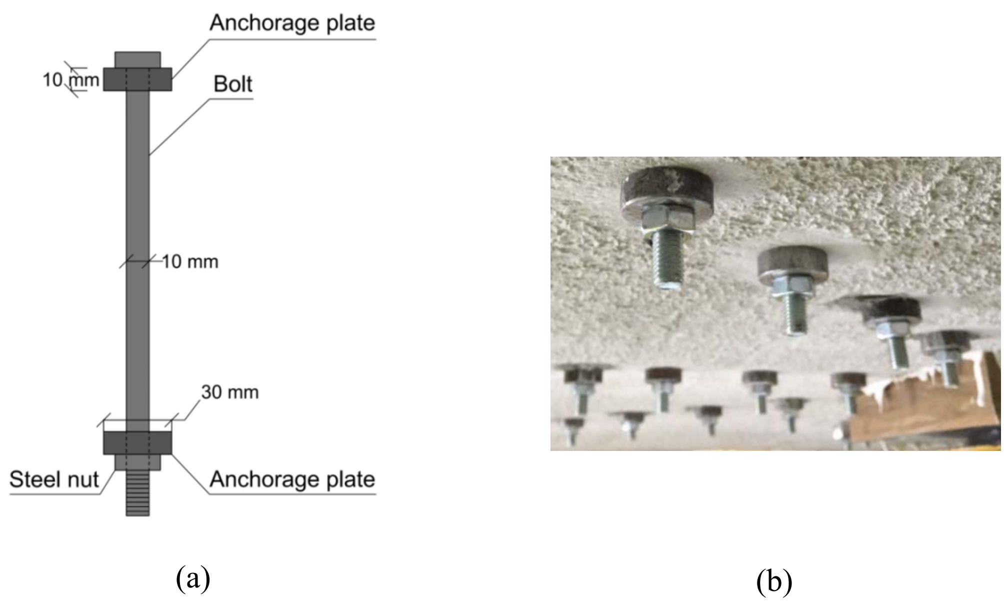

Fig.6 Steel shear bolts; (a) sketch of bolt and anchorage plates; (b) view of bolts from under the slab

The effectiveness of the EBROG technique compared to the EBR method in two FRP-strengthening configurations (i.e., covering the slab center with CFRP sheets and strengthening the region around the column) was investigated in the current study. Accordingly, one reference specimen, REF-B, and four CFRP-strengthened specimens with the following specifications were tested:

- Specimen EBR-CR-B was strengthened with two 150-mm-wide and 2180-mm-long strips in each direction, each consisting of two layers of CFRP sheets, as shown in Fig.4a. The configuration used in this specimen is applicable in cases that the column does not continue on the top of the slab, as in a building roof or a bridge deck. The term CR in the name of the specimen designates the cross configuration of the CFRP sheets. The strengthening technique used for this specimen was the conventional EBR method, in which the weak layer of concrete was removed by means of a grinding machine equipped with an abrasive stone (Fig. 7a), and after cleaning the surface from dust, the CFRP sheets were bonded on the substrate with epoxy resin (Fig.4b).
- Specimen EBROG-CR-B was strengthened with the same configuration as in EBR-CR-B, but the EBROG technique was employed for CFRP strengthening (Fig.4a and 4c). In this technique, surface preparation was accomplished through cutting six longitudinal grooves with 10 mm width, 10 mm depth, and 2180 mm length in the concrete cover in each direction, by means of a grinding machine with a cut-off disc (Fig. 7b), and cleaning the inside of the grooves and the concrete surface from dust. Afterward, the grooves were fully filled with epoxy resin and a layer of epoxy was applied on the substrate. The CFRP sheets were then adhered on the substrate and saturated completely with epoxy.

- Specimen EBR-GR-B received six strips of two-plies CFRP sheets in each direction, each 50 mm wide and 2180 mm long, around the column with the configuration shown in Fig.5a. This configuration corresponds to middle floor levels in a multi-storey building, where the column is continuous below and above the slab. The term GR in the specimen designation represents the grid-shape configuration of the CFRP sheets. The EBR method was used to apply the CFRP in this specimen (Fig.5b).
- Specimen EBROG-GR-B was strengthened similarly to EBR-GR-B, but using the EBROG technique instead of the EBR method. Six grooves 10-mm-wide, 10-mm-deep, and 2180-mm-long were cut in the concrete cover in each direction so that each CFRP strip was placed on one groove (Fig.5c) and adhered with the same procedure described for specimen EBROG-CR-B.

It should be mentioned that the strengthening procedures in the sequence described in this section, are applicable in practice.

(a) (b)

Fig. 7 Surface preparation; (a) in EBR method; (b) in EBROG method

2.4 Instrumentation

Five pairs of strain gauges (S1 to S10) were attached to five top reinforcement bars at the locations shown in Fig.8a. Each pair consists of two strain gauges glued at mid-height of the instrumented bar at two opposite locations on its diameter. Six strain gauges (F1 to F6) were glued on six points of the CFRP composite in places indicated in Fig.8b for specimens with different configurations. As shown in Fig.8a, the vertical deflections of the specimens were measured at eleven points along the orthogonal central lines using displacement transducers (D1 to D11).

3 Experimental results

3.1 Crack development and failure of the specimens

Initial damage to the reference specimen, REF-B, occurred in the form of tension cracks at the center of the slab in radial and circumferential directions. As the load increased, the cracks propagated extensively in the radial direction while the cracks in the central region and nearly parallel to the flexural steel reinforcement were much wider and extended almost to the full depth of the slab (Fig.9a). Such an extensive spread of tension cracks resulted in significant slab deformation and caused a ductile flexural failure mode of the specimen.

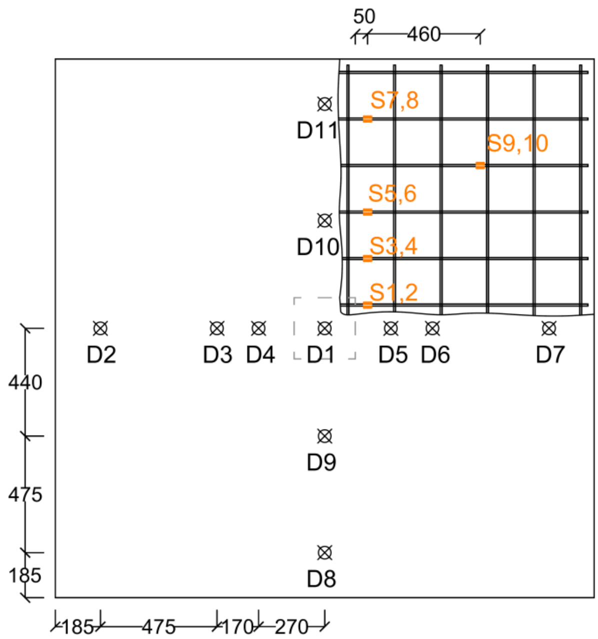

(a)

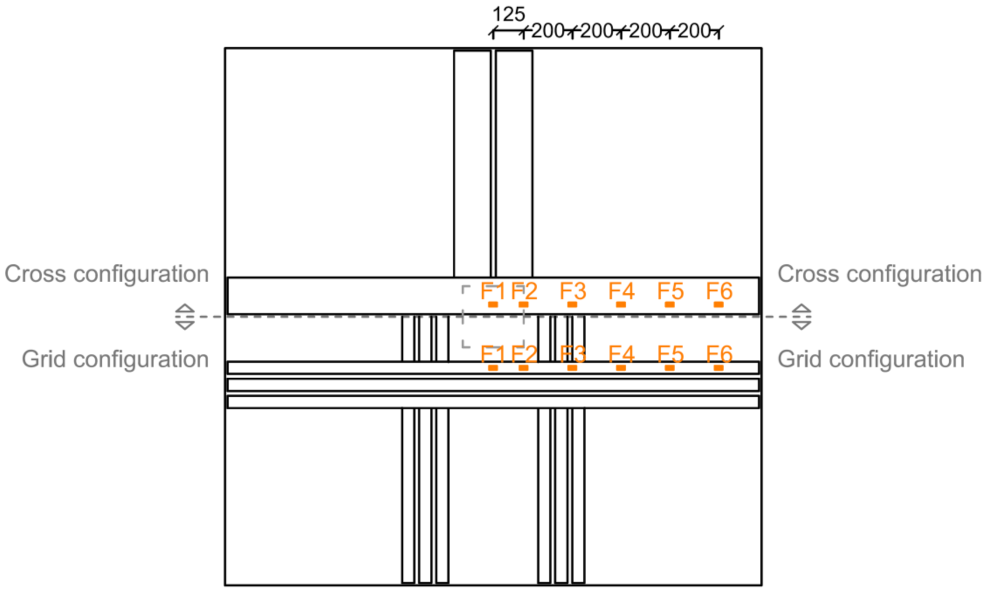

(b)

Fig.8 (a) Location of displacement transducers and strain gauges on rebars; (b) location of strain gauges on CFRP composites in cross and grid configurations (dimensions in mm)

Specimen EBR-CR-B failed by debonding of the CFRP sheets off the concrete substrate. Tension cracks with similar patterns to that of REF-B were observed in EBR-CR-B. Fig.9b shows the debonded CFRP sheets and the wide cracks underneath. The specimen EBROG-CR-B also failed by debonding of CFRP sheets; however, debonding was significantly postponed as a result of employing the EBROG technique in this specimen. As can be observed in Fig.9c, the CFRP composites debonded with thick pieces of concrete adhered to them while the underlying concrete was considerably spalled. Postponement of debonding in EBROG technique can be justified by the fact that applying CFRP sheets on grooves filled with epoxy led to an increase in the contact area between FRP and concrete substrate and caused the interfacial stresses to be transferred to the strong underlying concrete layers.

Debonding failure was also experienced by the specimens with CFRP sheets with a grid-shape configuration, i.e. EBR-GR-B and EBROG-GR-B. As in the case of the specimens with a cross configuration of the CFRP strengthening, debonding was postponed in the specimen in which EBROG technique was used, i.e. EBROG-GR-B.

Debonding in the specimen EBR-GR-B (with grid configuration) occurred at a higher load level than in the specimen EBR-CR-B (with cross configuration). Accordingly, although the EBROG technique was quite effective in postponing debonding in the grid configuration, its superiority over the EBR method was less significant compared to the case of the cross layout of CFRP strengthening. Fig.9d and e show the debonding and tension cracking of specimens EBR-GR-B and EBROG-GR-B, respectively. It can be observed that tension cracks in the central region nearly parallel to the steel reinforcement were the widest ones, extended through almost the full depth of the slab, similar to what was observed in the reference specimen.

(a)

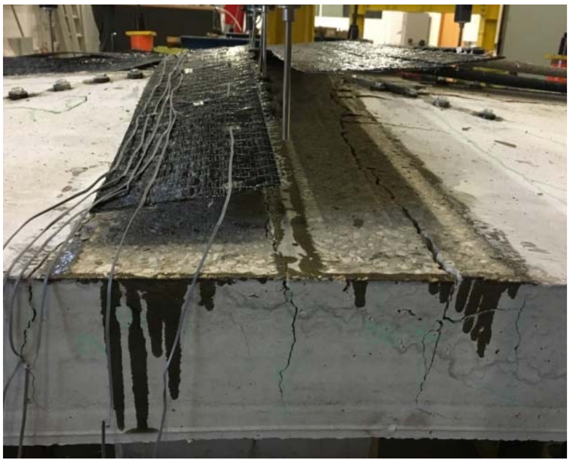

(b)

(c)

(d)

(e)

Fig.9 Test specimens after failure; (a) specimen REF-B; (b) specimen EBR-CR-B; (c) specimen EBROG-CR-B; (d) specimen EBR-GR-B; (e) specimen EBROG-GR-B

3.2 Load-deflection curves

The deflection was measured at the center of the slab as the difference between the measurement of the displacement transducer D1 and the average reading of displacement transducers D2 and D7 (see Fig.8a), where D2 and D7 are along the weak direction of the slab (the direction along which the effective depth of the flexural bars is smaller). The load is taken as the sum of the readings from the eight load cells installed at the perimeter of the specimen and the self-weight of the specimen and equipment. A summary of the main test results for all the specimens is presented in Table 3. The cracking and peak loads shown in the table are estimated based on the load-deflection curves, which are presented in Fig.10 for all the specimens. The deflection at peak load is also presented in Table 3 for each specimen. Finally, the table contains the deformation energy up to failure, calculated as the area under the load-deflection curve up to the point corresponding to the peak load.

Table 3 Summary of test results

Specimen	Cracking load (kN)	Peak load (kN)	Increase in peak load (%) compared to REF-B	Deflection at peak load (mm)	Deformation energy capacity (MN.mm)
REF-B	81.2	177.4	-	77.6	12.01
EBR-CR-B	106.8	180.2	2	11.0	1.66
EBROG-CR-B	110.2	245.8	39	20.5	4.09
EBR-GR-B	100.3	212.5	20	17.6	3.04
EBROG-GR-B	101.6	243.6	37	21.4	4.06

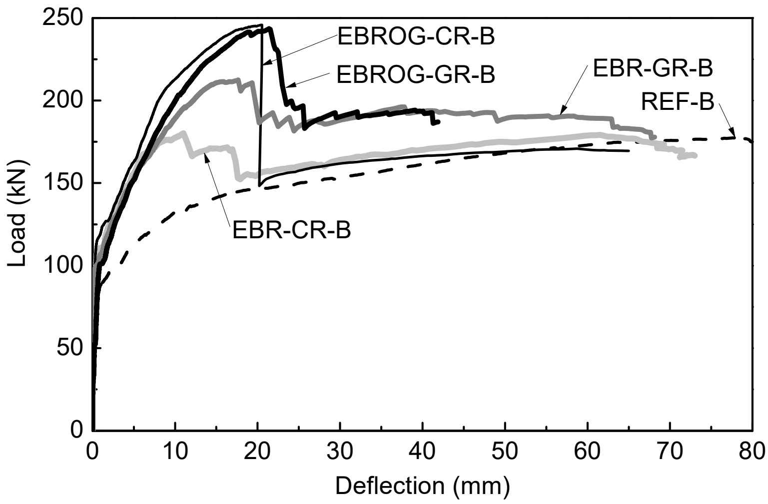

Fig.10 Load-deflection curves

Fig.10 shows that the reference specimen, REF-B, was characterized by a ductile behavior governed by flexure. The presence of punching shear strengthening through post-installed shear bolts effectively resulted in preventing punching shear failure of the specimen. The maximum load capacity of specimen REF-B was 177.4 kN. Flexural strengthening of this specimen was sought to increase its load-carrying capacity.

As previously described (Section 2), flexural strengthening was performed by gluing CFRP sheets on the tensile face. Fig.10 shows that CFRP strengthening resulted in a significant change in the behavior of the specimens. It is noticed that the specimens had comparable stiffness up to a certain point. The first to deviate from the group was specimen REF-B, which was the first to crack and to behave nonlinearly. The stiffness of specimen REF-B changed significantly from that of the CFRP strengthened specimens after this point. In the strengthened specimens, the load continued to increase with a comparable rate (stiffness).

The first FRP strengthened specimen to deviate from the group was EBR-CR-B. At a load level of 180.2 kN, this specimen suffered from debonding of the FRP, after which the load dropped to the level of specimen REF-B. This premature debonding in EBR-CR-B hindered the efficiency of the FRP strengthening, which resulted in a negligible load capacity increase by only 2%. The next specimen to deviate from the group was EBR-GR-B, in which the strengthening method was similar to EBR-CR-B but FRP composites were attached outside the column region. Despite the strengthening method being similar to that applied in EBR-CR-B, strengthening resulted in more effective in specimen EBR-GR-B, with a load capacity increase of 20%. Debonding occurred in this specimen for a higher load level.

The two specimens in which the EBROG method was used for bonding the FRP sheets behaved the most effectively. Specimens EBROG-CR-B and EBROG-GR-B had a load-carrying capacity increase of 39% and 37%, respectively. Furthermore, Fig.10 shows that the load-deflection curve of these two specimens was comparable for all levels of loading up to the peak load. In these specimens, debonding was efficiently postponed by enhancing the bond between FRP and concrete as a result of using the EBROG method. Comparing the efficiency of EBR and EBROG in the two different layouts of CFRP sheets (cross and grid forms), the load capacity was increased by 36% from EBR-CR-B to EBROG-CR-B and by 15% from EBR-GR-B to EBROG-GR-B. Accordingly, the EBROG technique proved more successful over EBR in postponing debonding in the case where the CFRP sheets were bonded in the cross layout.

The deflections at peak load were significantly different between the CFRP strengthened specimens and the reference one. A significantly stiffer behavior was observed in the specimens with CFRP strengthening, resulting in an average 90% decrease of the deflection at the maximum load level experienced by REF-B (177.4 kN). More specifically, the deflection for a load level of 177.4 kN was reduced from

77.6 mm in REF-B, to 6.2-10.0 mm in the CFRP strengthened specimens. This indicates that strengthening with CFRP, either in cross or grid layout, can be effective in mitigating serviceability issues in flat slabs. Furthermore, it is interesting to notice from Fig.10 that the load-deflection curves for all the CFRP strengthened specimens were almost identical for the range of load values experienced by specimen REF-B.

On the downside, the behavior of the CFRP strengthened specimens was significantly more brittle than that of the reference specimen REF-B. Fig.10 shows that there was a sudden drop in the load-carrying capacity of the strengthened specimens after reaching the peak load, providing little notice in case of accidental overloading. The brittleness of the CFRP strengthened flat slabs is also reflected in the low values of the deformation energy capacity in Table 3 compared to the reference specimen. Depending on the deflection at which CFRP debonding occurred, the deformation energy capacity of the strengthened specimens varied from nearly 14% to 34% of the deformation energy capacity of the reference specimen. Fig.10 shows also that the post-peak load-carrying capacity was higher in the specimens in which the GR configuration was used. This is explained by the fact that debonding did not occur simultaneously in all the CFRP sheets in these specimens (refer for example, to Fig.9d and 9e, where it can be noticed that bonded CFRP sheets remained in the vicinity of the column after debonding of sheets on the opposite location). On the contrary, when the CR configuration was used, debonding resulted in a complete loss of the benefits due to CFRP, and the post-peak behavior dropped to the levels of the reference specimen (Fig.10).

Regarding the overall behavior of the CFRP-strengthened specimens, especially their load-carrying capacity, specimens EBROG-GR-B and EBROG-CR-B presented the best performance.

3.3 Reinforcement strains

Fig.11 shows the readings of the strain gauges installed in flexural reinforcement bars as a function of the applied load. The labels of the strain gauges are shown in Fig.8a. Since two strain gauges were installed in the same bar, the post-processed average value is displayed in Fig.11. The graphs are interrupted at the point at which the readings become unreliable (for example, when the reading suddenly goes to zero or a very large value when a crack intercepts the strain gauge or when the strain gauge debonds). The horizontal dashed line represents the yielding strain.

Fig.11 shows that strains in the flexural reinforcement bars were low up to the load level corresponding to cracking (refer to Fig.10). Afterward, a rapid increase of the strains with the load is observed in all the specimens. A tendency to have lower strains with the increase of distance from the slab's center is observed, although the strains in S1/2 are in some cases lower than the strains measured by S3/4.

Yielding of the flexural reinforcement was detected at points near the column, as shown in Fig.11. Comparing the reference specimen with the other specimens, however, it is noticed that the first yield was postponed in the CFRP strengthened specimens. Furthermore, the first yield was postponed further by employing the EBROG method (compare for example EBR-CR-B with EBROG-CR-B in Fig.11).

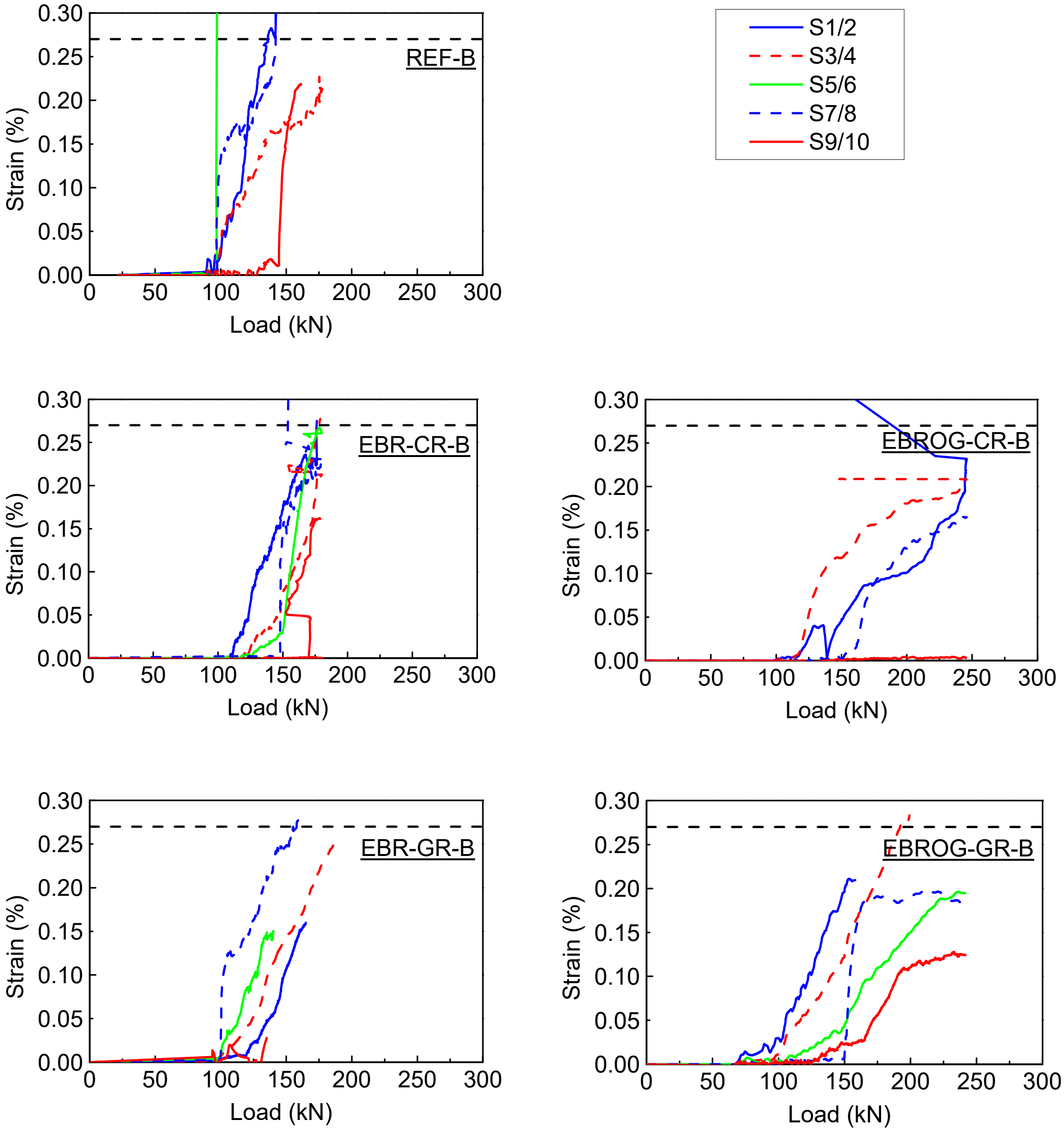

Fig.11 Strains in flexural reinforcement

3.4 Strains in FRP

Fig.12 and Fig.13 show the strains in FRP as a function of the applied load. The layout and names of the strain gauges used in these figures are shown in Fig.8b. Note that, due to the differences in the layout of the CFRP composites, the distance of the strain gauges from the slab's center is also different (Fig.8b).

In the specimens with the cross CFRP strengthening layout (CR) (Fig.12), there is a clear reduction of the strains with distance from the center of the slab. In these specimens, the highest strains are detected in the F1 strain gauges. In the specimen EBR-CR-B, the maximum recorded strain was 0.55% (equal to 31% of the FRP rupture strain), whereas a much higher value, equal to 0.96% (equal to 54% of the FRP rupture strain), was detected at the same location (F1) in the specimen with enhanced FRP bonding properties, EBROG-CR-B. Besides the low level of utilization of the capacity of the CFRP composites in the region near the column, Fig.12 indicates that the level of utilization was close to zero at the location of strain gauges F4 to F6 until debonding started. The initiation of debonding was associated with a rapid increase of the strains in F4 to F6, offering limited additional resistance for the specimen. In contrast, strains were significantly higher in F4 to F6 in specimen EBROG-CR-B at load levels near the peak load, demonstrating a higher level of utilization of the resistance of the CFRP composites all over the specimen.

In the specimens with the grid CFRP layout (GR) (Fig.13), the maximum recorded strain was 0.62% (equal to 35% of the FRP rupture strain) at F2 in specimen EBR-GR-B and 0.91% (equal to 51% of the FRP rupture strain) in F2 in EBROG-GR-B. Comparing the strain gauge readings for specimens with CR layout with those of specimens with the GR layout, it is observed that comparable levels of maximum strains were obtained for the same method of bonding the FRP (i.e., comparing EBR-CR-B with EBR-GR-B and comparing EBROG-CR-B with EBROG-GR-B). However, in specimens with the GR layout, the strains in F1 and F2 are comparable (unlike in the case of CR layout, where F2 strains are notably lower than those in F1). In specimen EBROG-GR-B, a high degree of utilization was detected.

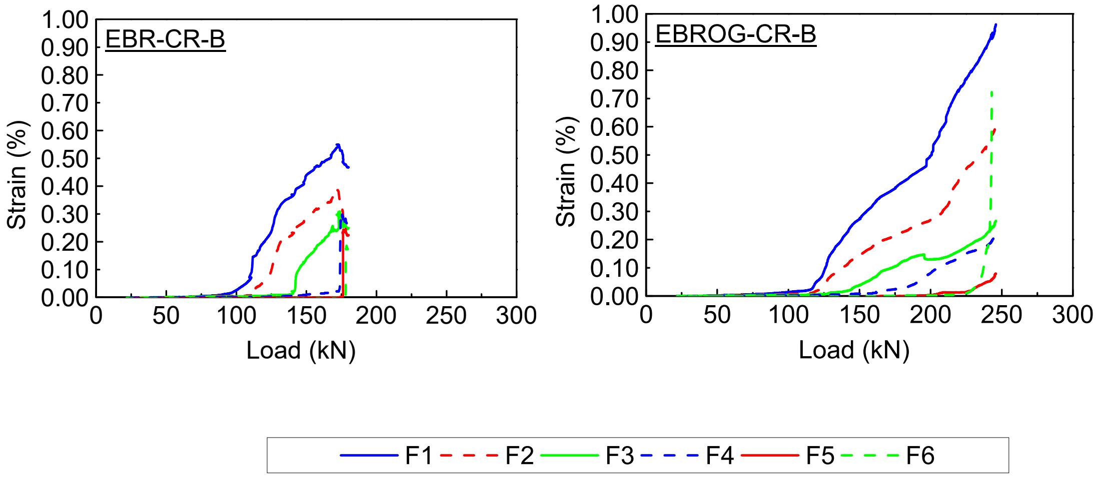

Fig.12 Strains in FRP for specimens with the CR layout

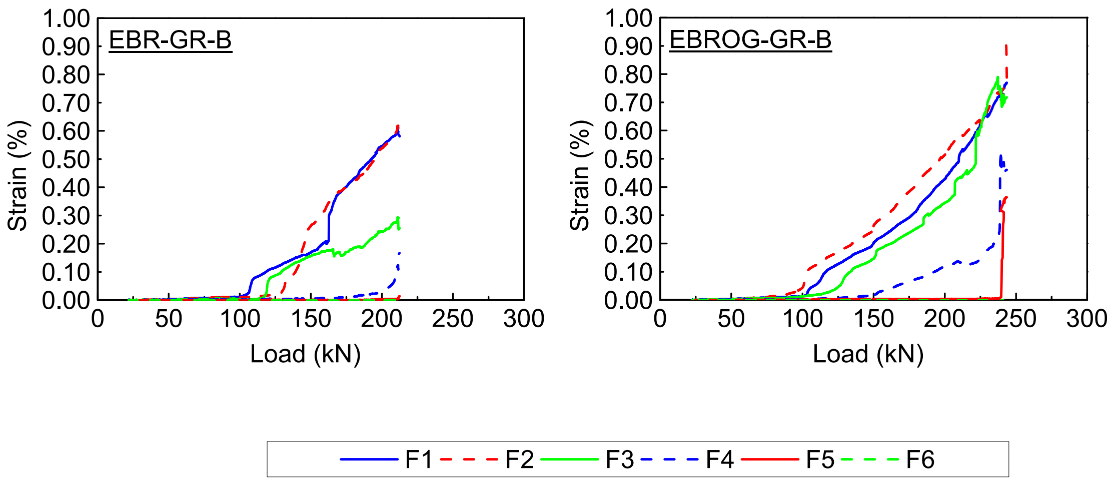

Fig.13 Strains in FRP for specimens with the GR layout

Comparing EBR with the EBROG method, it is clear from Fig.12 andFig.*13* that the maximum strains were considerably higher in specimens in which the EBROG method was used, regardless of the layout of the CFRP strengthening. This means that the method is effective in postponing debonding in CFRP strengthened flat slabs. Nonetheless, the maximum strains remained below the rupture strain of FRP.

Based on the test observations, the EBROG technique exhibited a better performance in enhancing the load capacity of slabs and in the utilisation of strain capacity of the FRP, compared to the EBR method. The superiority of the EBROG technique over the EBR method, proven for flexural strengthening of flat slabs in this study, was reported in the previous studies (e.g. [38–45]) for other cases of structural members.

Although no anchorage system, such as steel end anchor plates [28], transverse FRP anchorages [20,22], and steel bolts [29,30], was provided for the CFRP sheets in this study, significant improvement in the load capacity of the slab and high utilisation of the FRP strain capacity was achieved while employing the EBROG technique. This occurs because of the performance of the longitudinal grooves, which postpone the FRP debonding by transferring the interfacial stresses to the strong underlying concrete layers.

As a result, the EBROG technique is recommended to be used in practice when the flexural strengthening of a flat slab is required, provided that FRP strengthening is possible (for example, when adequate fire protection is applied).

4 Debonding strain

Extensive research on the EBR method has led to the development of a variety of FRP-concrete bond strength models (e.g. [48–56]), some of which are employed by different codes to evaluate the FRP-concrete bond strength. Table 4 summarizes the expressions suggested by ACI 440.2R [31], fib Bulletin 14 [57], and Japan Society of Civil Engineers (JSCE) [58] to calculate the debonding strain of externally bonded FRP composites. Using these expressions, the codes determine limitations for FRP strain to prevent an intermediate crack-induced debonding failure mode in an FRP-strengthened member [31,57,58]. In these formulas, f_c and f_{ct} are the compressive and tensile strength of concrete and E_f is the tensile modulus of elasticity of FRP. The terms n and t_f in the formulas suggested by ACI 440.2R and JSCE are the number of plies of FRP strengthening system and the nominal thickness of one ply of FRP, respectively. t_F in the formula of fib-bulletin 14 is the total thickness of FRP. The quantity ε_{fu} is the design rupture strain of FRP. The parameter G_f is the interfacial fracture energy which is recommended by JSCE [58] to be considered as 0.5 N/mm in absence of experimental results. It should be noted that site laminating of fibre sheets may produce fibre misalignment and also damage to the fibres due to the application process. It is therefore recommended by the manufacturer that the tensile modulus of elasticity used for the fibres be reduced by a reduction factor equal to 1.2 for design purposes [59]. Taking this recommendation into account, as well as the value of G_f as 0.5 N/mm, the values of the debonding strain based on the aforementioned codes are calculated and displayed in Table 4.

As shown in Section 3.4, the maximum strain of FRP sheets before debonding was 0.55% and 0.62% in specimens EBR-CR-B and EBR-GR-B, respectively. The comparison of these values with those obtained from the codes' formulas (presented in Table 4) shows that ACI 440.2R overestimates the debonding strain for the cases considered in this study, whereas the debonding strains estimated by fib Bulletin 14 and JSCE are lower than the values measured by the strain gauges.

Table 4 Debonding strains based on ACI 440.2R [31], fib Bulletin 14 [57], and JSCE [58]

Code	Suggested formula for debonding strain, ε_{fd} (%)	Debonding strain based on code's formula (%)
ACI 440.2R	$0.41\sqrt{f_c/nE_f t_f} \leq 0.9\varepsilon_{fu}$	1.02
fib-bulletin 14	$0.23\sqrt{\sqrt{f_c f_{ct}}/E_f t_F}$	0.30
JSCE	$\sqrt{2G_f/nE_f t_f}$	0.39

The maximum strain values recorded by strain gauges before debonding in specimens EBROG-CR-B and EBROG-GR-B were 0.96% and 0.91%, respectively. Compared to the code values in Table 4, the experimental value of the debonding strain when the EBROG technique is used is significantly higher than the values suggested by fib Bulletin 14 and JSCE; however, it is close to the value obtained using the expression of ACI 440.2R. It should be noted that the strain gauges were glued discretely to six points of the CFRP composite (F1 to F6 in Fig.8); the strain results are therefore local. Nevertheless, the load-strain curves shown in Fig.12 andFig.*13* represent rational and consistent strain values in the CFRP composites, supporting the observations discussed above regarding the debonding strains from the codes.

Besides various expressions and analytical models presented by different references for the debonding of externally bonded FRP reinforcement, there are various models in the literature to evaluate the debonding strength and strain for NSM FRP applications [49,60–64]. According to ACI 440.2R [31], the value of debonding strain for NSM reinforcement may vary from $0.6\varepsilon_{fu}$ to $0.9\varepsilon_{fu}$, depending on member specifications, including dimensions, steel and FRP reinforcement ratios, and surface roughness of the FRP rod.

Seracino et al. [49] developed a generic equation for intermediate crack-induced debonding resistance of EBR and NSM reinforcement, P_{IC}, as follows:

$$P_{IC} = 0.85\alpha_p \left(\frac{d_f}{b_f}\right)^{0.25} f_c^{\,0.33} \sqrt{L_{per}(EA)_p} < f_{rupt}A_p \qquad (1)$$

where, α_p is taken as 1.0 to obtain the mean value of P_{IC}, and is taken as 0.85 for the characteristic value of P_{IC}. L_{per} is the length of a debonding failure plane assumed to be 1 mm from the FRP composite. This failure plane is shown for EBR and NSM applications in Fig.14a and 14b, respectively. Parameters d_f and b_f are the length of the failure plane perpendicular and parallel to the concrete surface, respectively. $(EA)_p$ is the axial rigidity of the FRP plate, A_p is the cross-sectional area of the plate, and f_{rupt} is the FRP rupture stress. f_c is the compressive strength of concrete. The debonding strain may be obtained by dividing P_{IC} by the elastic modulus and cross-sectional area of FRP. It should be mentioned that Fig.14a and 14b are drawn not-to-scale for clarity purposes.

The test specimens in this study were strengthened with FRP sheets externally bonded on the concrete surface or on the grooves filled with epoxy. Regarding the two cases covered by the analytical model suggested by Seracino et al. [49], i.e. EBR and NSM reinforcement, this model is applicable in this study for specimens EBR-CR-B and EBR-GR-B by considering the failure plane shown in Fig.14a. Based on the model, the FRP debonding strains for EBR-CR-B and EBR-GR-B are obtained as 0.36% and 0.48%, respectively. Comparing these values with the experimental maximum strains 0.55% recorded for EBR-CR-B and 0.62% measured for EBR-GR-B, it is clear that the analytical values are lower than the experimental ones, indicating that the calculation based on the Seracino et al. [49] model is on the safe side.

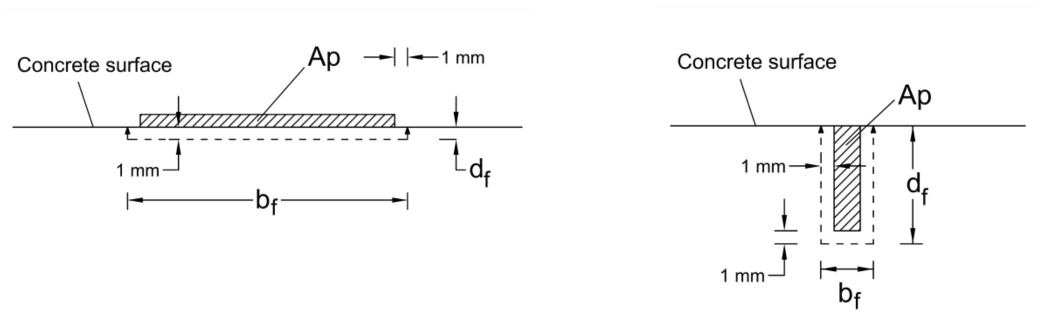

(a) (b)

Fig.14 Failure planes suggested by Seracino et al. [49] to estimate FRP debonding strain in different strengthening systems; (a) in EBR application; (b) in NSM application

An empirical model for estimating the intermediate crack-induced debonding resistance in the case of EBROG was recently developed for the first time by Moghaddas and Mostofinejad [65] by conducting 136 single lap-shear tests, and using nonlinear regression on the experimental results. Moghaddas and Mostofinejad [65] used Chen and Teng [48] model, which is one of the most accurate models for predicting EBR bond strength, as the starting point to estimate the EBROG bond strength. The Chen and Teng [48] model proposed the following expressions to estimate the ultimate bond strength $P_{Chen\&Teng}$:

$$P_{\mathrm{Chen}\,\&\,Teng} = 0.427\beta_p\beta_l\sqrt{f_c}b_fL_e \tag{2a}$$

$$\beta_p = \sqrt{\frac{2 - b_f/b_c}{1 + b_f/b_c}} \tag{2b}$$

$$L_e = \sqrt{\frac{E_f t_f}{\sqrt{f_c}}} \tag{2c}$$

$$\beta_l = \begin{cases} 1, & L \geq L_e \\ \sin\frac{\pi L}{2L_e}, & L < L_e \end{cases} \quad (2d)$$

where, b_f, t_f, and E_f are the width, thickness, and elasticity modulus of FRP sheets, respectively. b_c is the width of the concrete member and f_c is the compressive strength of concrete. L_e is the effective bond length proposed by Chen and Teng [48] to be calculated by Eq. (2c).

Moghaddas and Mostofinejad [65] modified the Chen and Teng [48] model by including a coefficient named as β_g to take the effect of grooving into account. Accordingly, the EBROG bond strength proposed by Moghaddas and Mostofinejad [65] is as follows:

$$P_{EBROG} = \beta_g P_{Chen\,\&\,Teng} \quad (3a)$$

$$\beta_g = {f_c}^{-0.33}(E_f t_f)^{-0.08}(8.1 - 0.006{h_g}^2 + 0.1h_g + 0.04b_g) \quad (3b)$$

where, h_g and b_g are the height and width of the grooves, respectively.

Using Eqs. (2a) through (2d) to calculate $P_{Chen\&\,Teng}$ for the test specimens strengthened via the EBR method in this study, and dividing $P_{Chen\&\,Teng}$ by the elastic modulus and cross-sectional area of FRP resulted in a value of 0.54% for the FRP debonding strain. Comparing this value with the maximum strain values recorded by the strain gauges, i.e. 0.55% and 0.62% for specimens EBR-CR-B and EBR-GR-B, respectively, shows that the Chen and Teng [48] model's estimation is very close to the experimental results in this study. Calculating P_{EBROG} by using Eq. (3a) and Eq. (3b) for the test specimens strengthened with the EBROG technique and dividing P_{EBROG} by the elastic modulus and cross-sectional area of FRP resulted in a value of 0.74% for the debonding strain. This value is lower than the maximum experimental values of 0.96% and 0.91% in specimens EBROG-CR-B and EBROG-GR-B, respectively, showing that the calculation is on the safe side.

According to the above discussion, the expressions proposed by fib Bulletin 14 [57] and JSCE [58] were on the safe side in estimating the debonding strain of the FRP sheets bonded with the EBR method, while the expression proposed by ACI 440.2R [31] overestimated the debonding strain. The calculation based on the Seracino et al. [49] model was also on the safe side. Chen and Teng [48] model's estimation was less than, but very close to the experimental results. Therefore, all the above references, except ACI 440.2R, are recommended in designing the externally bonded FRP strengthening system to be used in practice. For EBROG applications, the Moghaddas and Mostofinejad [65] model estimated the debonding strain on the safe side and is thus recommended for calculating the debonding strain for design purposes.

5 Load capacity prediction

Failure of all the specimens was governed by flexure. As a result, the load capacity can be predicted using the flexural strength, V_{flex}, which can be estimated using a yield-line analysis. An appropriate yield-line pattern for a uniformly reinforced slab with the geometry and boundary conditions of Fig.2 is shown in Fig.15 (according to Guandalini et al. [66]), dividing the slab into eight regions. Employing the yield-line analysis method results in the following equation for V_{flex} [66]:

$$V_{flex} = \frac{4m_R}{r_q\left(\cos\frac{\pi}{8} + \sin\frac{\pi}{8}\right) - c} \cdot \frac{B^2 - Bc - c^2/4}{B - c} \tag{4}$$

where, B, c, and r_q are the side dimension of the square slab, the square column size, and the radius of load introduction at the perimeter, as illustrated in Fig.15. The quantity

m_R is the nominal moment capacity of the slab per unit width. Eq. (4) was used in this study to estimate V_{flex} for specimen REF-B.

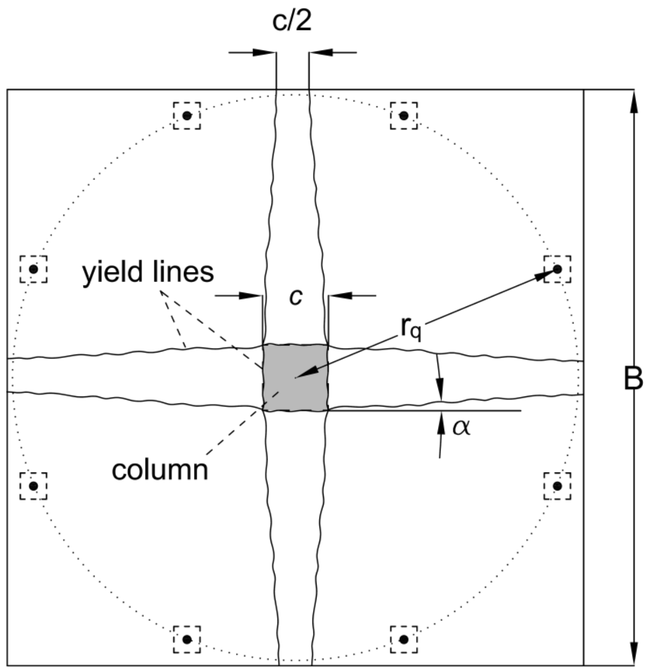

Fig.15 Yield-line pattern considered for the test specimens

An approach based on the yield-line analysis is suggested in this study to compute V_{flex} for the test specimens strengthened with CFRP sheets. In this approach, the yield-line pattern shown in Fig.15 was considered according to the test observations. The yield-line analysis was used to calculate V_{flex} corresponding to given plastic moment resistance in various parts of the slab. The plastic moment resistances are the nominal moment capacities per unit width of a slab section with the reinforcement layers, i.e. flexural steel reinforcement and CFRP sheets, crossed by the yield lines. Therefore, the first step in this approach is to distinguish the location of CFRP composites with respect to the yield lines in order to determine the reinforcement layers which are crossed by the yield lines. Accordingly, two different nominal moment capacities per unit width m_R

and $m_{R,FRP}$ are used in this approach for the parts without FRP strengthening and for the CFRP-strengthened parts, respectively.

The bending moment, m_b, and the twisting moment, m_t, per unit length of a yield line crossing the CFRP composite at an angle α to the reinforcement, as shown in Fig.16, can be calculated as a function of m_R and $m_{R,FRP}$ from moment equilibrium.

$$m_b = m_R \cos^2\alpha + m_{R,FRP} \sin^2\alpha \tag{5a}$$

$$m_t = \frac{1}{2}\left(m_{R,FRP} - m_R\right)\sin 2\alpha \tag{b}$$

Giving the column a virtual displacement, δ, and equatingthe external work done by the concentric load with the sum of the separate internal works done by each plate region while rotating about the respective axis of rotation, V_{flex} is obtained as a function of m_R and $m_{R,FRP}$.

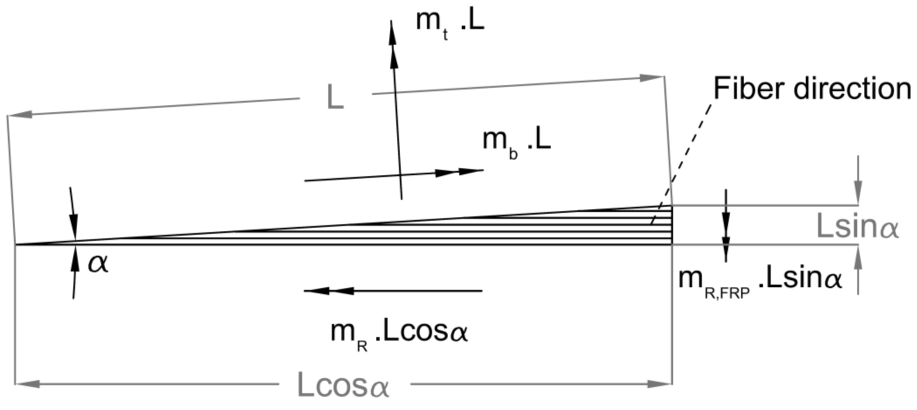

Fig.16 Moments of a yield line crossing the CFRP composite

It should be mentioned that $m_{R,FRP}$ was calculated on a trial-and-error basis by first assuming a value for the depth to the neutral axis and computing the strain profile (more specifically, strains at the level of steel reinforcement and at the extreme concrete compression fibre) by assuming that the strain at the FRP layer is equal to the debonding strain of FRP as determined from the strain gauge readingsduring the experiments and using strain compatibility. As a result of this assumption, the flexural resistance $m_{R,FRP}$ is limited by the debonding of FRP. The procedure for the calculation of $m_{R,FRP}$ continues by checking internal force equilibrium. When the equilibrium is not satisfied, the depth to the neutral axis is revised and the steps above are repeated. Otherwise, $m_{R,FRP}$ is calculated by establishing moment equilibrium.

Table 5 presents the values of V_{flex} calculated with the described approach. The experimental load-carrying capacities for the test specimens are also given in Table 5 for reference. It is observed that the load capacity of specimen REF-B is 22% higher than V_{flex} obtained by the yield-line analysis. According to previous studies, this difference can be attributed to strain-hardening of tensile reinforcement [67], second-order effects making the slab perform as a folded plate, tensile strength of plain concrete, etc. As discussed in [67], V_{flex} can deviate from the experimental load especially in lightly reinforced flat slabs, such as REF-B, which had a flexural reinforcement ratio of only 0.2%. For the CFRP-strengthened specimens, which were significantly stiffer, the ratio V_{exp}/V_{flex} shows that the employed approach predicts reasonably well the load capacity of these specimens. Accordingly, this simple approach can be used for design purposes to calculate the flexural capacity of FRP-strengthened slabs.

Table 5 Flexural strength versus experimental load capacity

Specimen	V_{exp} (kN)	V_{flex} (kN)	V_{exp}/V_{flex}
REF-B	177.4	145.1	1.22
EBR-CR-B	180.2	186.5	0.97
EBROG-CR-B	245.8	216.8	1.13
EBR-GR-B	212.5	202.8	1.05
EBROG-GR-B	243.6	228.7	1.07

6 Conclusions

The concentric loading tests of four CFRP strengthened flat slab specimens and a reference specimen without CFRP were described in this paper. Due to the presence of a relatively large amount of shear reinforcement, punching shear failure was prevented in all the specimens, allowing for a better study of the efficiency of the tested flexural strengthening solutions. The tested solutions resulted from the combination of two layouts of the CFRP sheets and two techniques (EBR and EBROG) for bonding the CFRP composites to the existing concrete substrate. The following conclusions canbe drawn from this study:

1. The experimental results showed that the EBROG technique is effective in postponing the debonding of CFRP composites used for the flexural strengthening of flat slabs. The debonding strainsweremuch higher in the case of EBROGcomparedto strains in the case of EBR. The maximum strain measured by the strain gauges was 0.55% and 0.62% in specimens EBR-CR-B and EBR-GR-B, respectively, while it was 0.96% and 0.91% in specimens EBROG-CR-B and EBROG-GR-B, respectively.

2. The superiority of the EBROG technique over the EBR method was proved in bothroof level slab-column connections and intermediate floor levels, where the column continuity does not allow the application of the CFRP sheets over the column region.The load capacity was increased by 36% from EBR-CR-B to EBROG-CR-B and by 15% from EBR-GR-B to EBROG-GR-B. This indicates that EBROG can be an efficient solution for the flexural strengthening of flat slabs in practice.
3. The differences in the layout of the CFRP sheets resulted in differences in the distribution of strains during the tests, but the overall and ultimate behavior of the specimens with cross and grid layouts of CFRP was comparable when the EBROG method wasused. Differences were found in the case of the use of the conventional EBR method, in which the grid layout performed better than the cross layout.
4. It was found that the expressions from fib Bulletin 14 [57] and Japan Society of Civil Engineers (JSCE) [58], intended for use in case of the EBR technique, resulted in debonding strains close to the experimentally measured values (but underestimated) in specimens in which the EBR technique was applied. ACI 440.2R [31], on the other hand, overestimated the debonding strain of the specimens presented in this paper, predictinga debonding strain close to the value observed in the specimens with enhanced bond properties (EBROG technique).
5. Prediction of the FRP debonding strain in the EBR applications based on the Seracino et al. [49] model was on the safe side. Using the Chen and Teng [48] model resulted in an analytical strain less than, but very close to the experimental strain. The Moghaddas and Mostofinejad [65] model, which is the only bond strength model developed for the EBROG applications, resulted in a debonding

strain lower than the experimentally recorded strains, indicating that the model prediction is on the safe side.

6. A simple approach based on yield-line theory and the experimentally observed debonding strains was presented to calculate the flexural capacity of the specimens.The approach predicted reasonably well the failure loads of the specimens strengthened with FRP.

Acknowledgment

The authors would like to thank the team members at the structural laboratory of the Department of Civil Engineering at Universidade NOVA de Lisboa. Research mobility grant received from the Iranian Ministry of Science, Research, and Technology (MSRT) and from Isfahan University of Technology (IUT) for the visiting research period of the first author at Universidade NOVA de Lisboa is highly acknowledged.

Conflict of interest

There is no conflict of interest.

Funding

This research did not receive any specific grant from funding agencies in the public, commercial, or not-for-profit sectors.

References

[1] Ghali A, Sargious MA, Huizer A. Vertical Prestressing of Flat Plates Around Columns. ACI Spec Publ 1974;42:905–20.

[2] Ruiz MF, Muttoni A, Kunz J. Strengthening of flat slabs against punching shear using post installed shear reinforcement. ACI Struct J 2010;107:434–42.

[3] Inácio MMG, Pinho Ramos A, Faria DMV. Strengthening of flat slabs with transverse reinforcement by introduction of steel bolts using different anchorage approaches. Eng Struct 2012;44:63–77. doi:10.1016/j.engstruct.2012.05.043.

[4] Silva R, Faria DMV, Ramos AP, Inácio M. A physical approach for considering how anchorage head size influences the punching capacity of slabs strengthened with vertical steel bolts. Struct Concr 2013;14:389–400. doi:10.1002/suco.201200051.

[5] Einpaul J, Brantschen F, Fernández Ruiz M, Muttoni A. Performance of punching shear reinforcement under gravity loading: Influence of type and detailing. ACI Struct J 2016;113:827–38. doi:10.14359/51688630.

[6] Wörle P. Enhanced shear punching capacity by the use of post installed concrete screws. Eng Struct 2014;60:41–51. doi:10.1016/j.engstruct.2013.12.015.

[7] Binici B, Bayrak O. Upgrading of slab–column connections using fiber reinforced polymers. Eng Struct 2005;27:97–107. doi:10.1016/j.engstruct.2004.09.005.

[8] Meisami MH, Mostofinejad D, Nakamura H. Punching shear strengthening of two-way flat slabs using CFRP rods. Compos Struct 2013;99:112–22. doi:10.1016/j.compstruct.2012.11.028.

[9] Meisami MH, Mostofinejad D, Nakamura H. Punching Shear Strengthening of Two-Way Flat Slabs with CFRP Grids. J Compos Constr 2014;18:04013047. doi:10.1061/(ASCE)CC.1943-5614.0000443.

[10] Meisami MH, Mostofinejad D, Nakamura H. Strengthening of flat slabs with

FRP fan for punching shear. Compos Struct 2015;119:305–14. doi:10.1016/j.compstruct.2014.08.041.

[11] Fernandes H, Lúcio V, Ramos A. Strengthening of RC slabs with reinforced concrete overlay on the tensile face. Eng Struct 2017;132:540–50. doi:10.1016/j.engstruct.2016.10.011.

[12] Lapi M, Fernandes H, Orlando M, Ramos A, Lúcio V. Performance assessment of flat slabs strengthened with a bonded reinforced-concrete overlay. Mag Concr Res 2017;70:433–51. doi:10.1680/jmacr.17.00037.

[13] Ebead U, Marzouk H. Strengthening of Two-Way Slabs Using Steel Plates. ACI Struct J 2002;99:23–31. doi:10.14359/11032.

[14] Babaeidarabad S, Loreto G, Nanni A. Flexural strengthening of RC beams with an externally bonded fabric-reinforced cementitious matrix. J Compos Constr 2014. doi:10.1061/(ASCE)CC.1943-5614.0000473.

[15] Loreto G, Babaeidarabad S, Leardini L, Nanni A. RC beams shear-strengthened with fabric-reinforced-cementitious-matrix (FRCM) composite. Int J Adv Struct Eng 2015;7:341–52. doi:10.1007/s40091-015-0102-9.

[16] Bournas DA, Triantafillou TC, Zygouris K, Stavropoulos F. Textile-Reinforced Mortar versus FRP Jacketing in Seismic Retrofitting of RC Columns with Continuous or Lap-Spliced Deformed Bars. J Compos Constr 2009;13:360–71. doi:10.1061/(ASCE)CC.1943-5614.0000028.

[17] Papanicolaou C, Triantafillou T, Papantoniou I, Balioukos C. Strengthening of two-way reinforced concrete slabs with Textile Reinforced Mortars (TRM). 4th

Colloq Text Reinf Struct 2009:409–20.

[18] Abbas H, Abadel AA, Almusallam T, Al-Salloum Y. Effect of CFRP and TRM Strengthening of RC Slabs on Punching Shear Strength. Lat Am J Solids Struct 2015;12:1616–40. doi:10.1590/1679-78251277.

[19] Koutas LN, Bournas DA. Flexural Strengthening of Two-Way RC Slabs with Textile-Reinforced Mortar: Experimental Investigation and Design Equations. J Compos Constr 2017. doi:10.1061/(ASCE)CC.1943-5614.0000713.

[20] Akhundzada H, Donchev T, Petkova D. Strengthening of slab-column connection against punching shear failure with CFRP laminates. Compos Struct 2019;208:656–64. doi:10.1016/j.compstruct.2018.09.076.

[21] Harajli MH, Soudki KA. Shear strengthening of interior slab-column connections using carbon fiber-reinforced polymer sheets. J Compos Constr 2003;7:145–53. doi:10.1061/(ASCE)1090-0268(2003)7:2(145).

[22] Ebead U, Marzouk H. Fiber-reinforced polymer strengthening of two-way slabs. ACI Struct J 2004;101:650–9.

[23] Limam O, Foret G, Ehrlacher A. RC two-way slabs strengthened with CFRP strips: Experimental study and a limit analysis approach. Compos Struct 2003;60:467–71. doi:10.1016/S0263-8223(03)00011-4.

[24] Kim YJ, Longworth JM, Wight RG, Green MF. Flexure of Two-Way Slabs Strengthened with Prestressed or Nonprestressed CFRP Sheets. J Compos Constr 2008;12:366–74. doi:10.1061/(ASCE)1090-0268(2008)12:4(366).

[25] Elsayed WE, Ebead UA, Neale KW. Mechanically Fastened FRP-Strengthened

Two-Way Concrete Slabs with and without Cutouts. J Compos Constr 2009;13:198–207. doi:10.1061/(asce)cc.1943-5614.0000004.

[26] Kim YJ, Longworth JM, Wight RG, Green MF. Punching Shear of Two-way Slabs Retrofitted with Prestressed or Non-prestressed CFRP Sheets. J Reinf Plast Compos 2010;29:1206–23. doi:10.1177/0731684409103143.

[27] Chen ZF, Wan LL, Lee S, Ng M, Tang JM, Liu M, et al. Evaluation of CFRP, GFRP and BFRP Material Systems for the Strengthening of RC Slabs. J Reinf Plast Compos 2008;27:1233–43. doi:10.1177/0731684407084122.

[28] Abdullah A, Bailey CG, Wu ZJ. Tests investigating the punching shear of a column-slab connection strengthened with non-prestressed or prestressed FRP plates. Constr Build Mater 2013;48:1134–44. doi:10.1016/j.conbuildmat.2013.07.012.

[29] El-Salakawy E, Soudki K, Polak MA. Punching Shear Behavior of Flat Slabs Strengthened with Fiber Reinforced Polymer Laminates. J Compos Constr 2004;8:384–92. doi:10.1061/(ASCE)1090-0268(2004)8:5(384).

[30] Harajli MH, Soudki KA, Kudsi T. Strengthening of Interior Slab–Column Connections Using a Combination of FRP Sheets and Steel Bolts. J Compos Constr 2006;10:399–409. doi:10.1061/(ASCE)1090-0268(2006)10:5(399).

[31] ACI Committee 440. Guide for the Design and Construction of Externally Bonded FRP Systems for Strengthening Concrete Structures. ACI 440.2R-17 2017:76.

[32] El-Hacha R, Rizkalla SH. Near-Surface-Mounted Fiber-Reinforced Polymer

Reinforcements for Flexural Strengthening of Concrete Structures. ACI Struct J 2004;101. doi:10.14359/13394.

[33] Bilotta A, Ceroni F, Nigro E, Pecce M. Efficiency of CFRP NSM strips and EBR plates for flexural strengthening of RC beams and loading pattern influence. Compos Struct 2015;124:163–75. doi:10.1016/j.compstruct.2014.12.046.

[34] Barros JAO, Ferreira DRSM, Fortes AS, Dias SJE. Assessing the effectiveness of embedding CFRP laminates in the near surface for structural strengthening. Constr Build Mater 2006;20:478–91. doi:10.1016/j.conbuildmat.2005.01.030.

[35] D'Antino T, Pisani MA. Evaluation of the effectiveness of current guidelines in determining the strength of RC beams retrofitted by means of NSM reinforcement. Compos Struct 2017;167:166–77. doi:10.1016/j.compstruct.2017.01.070.

[36] Bilotta A, Ceroni F, Di Ludovico M, Nigro E, Pecce M, Manfredi G. Bond Efficiency of EBR and NSM FRP Systems for Strengthening Concrete Members. J Compos Constr 2011;15:757–72. doi:10.1061/(ASCE)CC.1943-5614.0000204.

[37] Foret G, Limam O. Experimental and numerical analysis of RC two-way slabs strengthened with NSM CFRP rods. Constr Build Mater 2008;22:2025–30. doi:10.1016/j.conbuildmat.2007.07.027.

[38] Mostofinejad D, Mahmoudabadi E. Grooving as Alternative Method of Surface Preparation to Postpone Debonding of FRP Laminates in Concrete Beams. J Compos Constr 2010;14:804–11. doi:10.1061/(ASCE)CC.1943-5614.0000117.

[39] Mostofinejad D, Shameli M. Performance of EBROG Method under Multilayer

FRP Sheets for Flexural Strengthening of Concrete Beams. Procedia Eng 2011;14:3176–82. doi:10.1016/j.proeng.2011.07.401.

[40] Mostofinejad D, Tabatabaei Kashani A. Experimental study on effect of EBR and EBROG methods on debonding of FRP sheets used for shear strengthening of RC beams. Compos Part B Eng 2013;45:1704–13. doi:10.1016/j.compositesb.2012.09.081.

[41] Mostofinejad D, Moshiri N. Compressive Strength of CFRP Composites Used for Strengthening of RC Columns: Comparative Evaluation of EBR and Grooving Methods. J Compos Constr 2014;19:04014079. doi:10.1061/(asce)cc.1943-5614.0000545.

[42] Torabian A, Mostofinejad D. Externally Bonded Reinforcement on Grooves Technique in Circular Reinforced Columns Strengthened with Longitudinal Carbon Fiber-Reinforced Polymer under Eccentric Loading. ACI Struct J 2017;114:861–73. doi:10.14359/51689567.

[43] Mostofinejad D, Torabian A. Experimental Study of Circular RC Columns Strengthened with Longitudinal CFRP Composites under Eccentric Loading: Comparative Evaluation of EBR and EBROG Methods. J Compos Constr 2016;20:04015055. doi:10.1061/(ASCE)CC.1943-5614.0000618.

[44] Mostofinejad D, Akhlaghi A. Experimental Investigation of the Efficacy of EBROG Method in Seismic Rehabilitation of Deficient Reinforced Concrete Beam–Column Joints Using CFRP Sheets. J Compos Constr 2016;21:04016116. doi:10.1061/(asce)cc.1943-5614.0000781.

[45] Mostofinejad D, Hajrasouliha M. Shear Retrofitting of Corner 3D-Reinforced

Concrete Beam-Column Joints Using Externally Bonded CFRP Reinforcement on Grooves. J Compos Constr 2018;22:04018037. doi:10.1061/(asce)cc.1943-5614.0000862.

[46] S&P Clever Reinforcement Company. User guide; S&P C-Sheet 240, Unidirectional carbon fibre fabric for structural reinforcement 2018.

[47] S&P Clever Reinforcement Company. User guide; S&P Resin 55 HP, two-component epoxy resin adhesive 2018.

[48] Chen JF, Teng JG. Anchorage Strength Models for FRP and Steel Plates Bonded to Concrete. J Struct Eng 2001;127:784–91. doi:10.1061/(ASCE)0733-9445(2001)127:7(784).

[49] Seracino R, Raizal Saifulnaz MR, Oehlers DJ. Generic Debonding Resistance of EB and NSM Plate-to-Concrete Joints. J Compos Constr 2007;11:62–70. doi:10.1061/(ASCE)1090-0268(2007)11:1(62).

[50] Teng JG, Yuan H, Chen JF. FRP-to-concrete interfaces between two adjacent cracks: Theoretical model for debonding failure. Int J Solids Struct 2006;43:5750–78. doi:10.1016/j.ijsolstr.2005.07.023.

[51] Teng JG, Smith ST, Yao J, Chen JF. Intermediate crack-induced debonding in RC beams and slabs. Constr Build Mater 2003;17:447–62. doi:10.1016/S0950-0618(03)00043-6.

[52] Teng JG, Chen JF, Smith ST, Lam L. FRP: Strengthened RC Structures. West Sussex, UK: John Wiley & Sons; 2002.

[53] Lu XZ, Ye LP, Teng JG, Jiang JJ. Meso-scale finite element model for FRP

sheets/plates bonded to concrete. Eng Struct 2005;27:564–75. doi:10.1016/j.engstruct.2004.11.015.

[54] Wu Y, Zhou Z, Yang Q, Chen W. On shear bond strength of FRP-concrete structures. Eng Struct 2010;32:897–905. doi:10.1016/j.engstruct.2009.12.017.

[55] Wu Y-F, Xu X-S, Sun J-B, Jiang C. Analytical solution for the bond strength of externally bonded reinforcement. Compos Struct 2012;94:3232–9. doi:10.1016/j.compstruct.2012.04.026.

[56] Pan J, Wu Y-F. Analytical modeling of bond behavior between FRP plate and concrete. Compos Part B Eng 2014;61:17–25. doi:10.1016/j.compositesb.2014.01.026.

[57] fib - Task Group 9.3. fib Bulletin 14: Externally bonded FRP reinforcement for RC structures. vol. 14. Lausanne: 2001.

[58] Japan Society of Civil Engineers (JSCE). Recommendations for upgrading of concrete structures with use of continuous fiber sheets 2001:88.

[59] S&P. Basics for S&P FRP-Systems VER062018/IND 2018:34. https://www.sp-reinforcement.ch/sites/default/files/field_product_col_doc_file/basics_for_sp_frp-systems_e_ver062018_3.pdf (accessed May 1, 2019).

[60] Seracino R, Jones NM, Ali MSM, Page MW, Oehlers DJ. Bond Strength of Near-Surface Mounted FRP Strip-to-Concrete Joints. J Compos Constr 2007;11:401–9. doi:10.1061/(ASCE)1090-0268(2007)11:4(401).

[61] De Lorenzis, L., and La Tegola A. Analytical modeling of splitting bond failure for NSM FRP reinforcement in concrete. In: Tan KH, editor. Proc., 6th Int.

Symp. FRPRCS, Singapore: 2003, p. 975–984.

[62] Blaschko M. Bond behavior of CFRP strips glued into slits. In: Tan KH, editor. 6th Int. Symp. FRPRCS, Singapore: 2003, p. 205–214.

[63] De Lorenzis L, Lundgren K, Rizzo A. Anchorage Length of Near-Surface Mounted Fiber-Reinforced Polymer Bars for Concrete Strengthening - Experimental Investigation and Numerical Modeling. ACI Struct J 2004. doi:10.14359/13025.

[64] Hassan T, Rizkalla S. Investigation of Bond in Concrete Structures Strengthened with Near Surface Mounted Carbon Fiber Reinforced Polymer Strips. J Compos Constr 2003;7:248–57. doi:10.1061/(ASCE)1090-0268(2003)7:3(248).

[65] Moghaddas A, Mostofinejad D. Empirical FRP-Concrete Bond Strength Model for Externally Bonded Reinforcement on Grooves. J Compos Constr 2019;23:04018080. doi:10.1061/(ASCE)CC.1943-5614.0000924.

[66] Guandalini S, Burdet OL, Muttoni A. Punching tests of slabs with low reinforcement ratios. ACI Struct J 2009;106:87–95. doi:10.14359/56287.

[67] Torabian A, Isufi B, Mostofinejad D, Ramos AP. Behavior of thin lightly reinforced flat slabs under concentric loading. Eng Struct 2019;196:109327. doi:10.1016/j.engstruct.2019.109327.

Figure captions

Fig. 1 Unidirectional carbon fibre fabric S&P C-Sheet 240

Fig. 2 Geometry and steel reinforcement of test specimens (dimensions in mm)

Fig. 3 Test setup

Fig. 4 Specimens EBR-CR-B and EBROG-CR-B (dimensions in mm); (a) configuration of CFRP sheets and steel bolts; (b) section view in EBR-CR-B; (b) section view in EBROG-CR-B

Fig. 5 Specimens EBR-GR-B and EBROG-GR-B (dimensions in mm); (a) configuration of CFRP sheets and steel bolts; (b) section view in EBR-GR-B; (c) section view in EBROG-GR-B

Fig. 6 Steel shear bolts; (a) sketch of bolt and anchorage plates; (b) view of bolts from under the slab

Fig. 7 Surface preparation; (a) in EBR method; (b) in EBROG method

Fig. 8 (a) Location of displacement transducers and strain gauges on rebars; (b) location of strain gauges on CFRP composites in cross and grid configurations (dimensions in mm)

Fig. 9 Test specimens after failure; (a) specimen REF-B; (b) specimen EBR-CR-B; (c) specimen EBROG-CR-B; (d) specimen EBR-GR-B; (e) specimen EBROG-GR-B

Fig. 10 Load-deflection curves

Fig. 11 Strains in flexural reinforcement

Fig. 12 Strains in FRP for specimens with the CR layout

Fig. 13 Strains in FRP for specimens with the GR layout

Fig. 14 Failure planes suggested by Seracino et al. [49] to estimate FRP debonding strain in different strengthening systems; (a) in EBR application; (b) in NSM application

Fig. 15 Yield-line pattern considered for the test specimens

Fig. 16 Moments of a yield line crossing the CFRP composite